Heliyon 10 (2024) e30181

Contents lists available at ScienceDirect

Heliyon

journal homepage: www.cell.com/heliyon

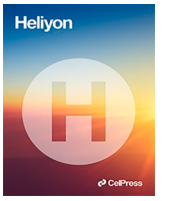

Research article

Tunability of domain structure in partially inverse spinels $NiAl_2O_4$

M. Arshad Farhan [a,*], Sadaf Javaid [a,b], Lubna Rasheed [c], M. Atiq Ur Rehman [d], M. Nadeem [a]

[a] Polymer Composite Group, Directorate of Science, PINSTECH, P.O. Nilore, Islamabad, Pakistan
[b] Department of Chemistry, University of Education, Attock Campus, Pakistan
[c] Department of Chemistry, Rawalpindi Women University, Rawalpindi, Pakistan
[d] Department of Materials Science and Engineering, Institute of Space Technology Islamabad, 44000, Pakistan

ARTICLE INFO

Keywords:
Cationic domains
Structure-Property Relationship
Chemical pressure perturbation
Cationic-rearrangement
Partially-inverse Spinel

ABSTRACT

Re-arrangement of cationic distribution in partially inverse spinel $NiAl_2O_4$ by using chemical pressure perturbation is studied. Structural, impedance and magnetic analysis suggest presence of regions/domains inside the grain/bulk with same lattice arrangement but varying in cationic oxidation state. Perturbing the cationic distribution in the grain via low concentrations of ambivalence substituent rearranges the cationic distribution across these domains within the partially inverse spinel lattice without disturbing the crystal structure. A comprehensive explanation on the origin & tunability of cationic distribution within the partially-inverse lattice is proposed.

1. Introduction

Complex oxide materials such as spinels are known for their unconventional yet exotic properties originating from their ordered/disordered structure [1–3]. These spinels consist of a combination of binary oxides with excellent photocatalytic, physicochemical, antimicrobial applications [4–7]. Transition metal Aluminates are an example of such spinels with tremendous importance [8–11]. The unique binary oxide system consisting on a combination of p-type (NiO) dispersed between the dielectric (Al_2O_3) generates remarkable electrical performance distinct from its constituents [12,13]. Owing to excellent thermal, chemical & mechanical stability & unique electro-optic characteristics, it has been under study for metal containing ceramic-composites, and radiation protection applications [14–20]. It has also been extensively deliberated for catalytic applications owing to its unique porous structure [21–24]. The most important claim for $NiAl_2O_4$ is its potential application as metamaterial owing to its distinctive dielectric response [25]. However, its permittivity response to incident AC frequency, Magnetic behavior and polarization & conduction mechanisms are not conclusive [26–29]. Such anomalies originate from the cationic distribution within partially-inverse spinel structure [12] which has an order-disordered face-centered cubic structure with *Fd3m* space group [30,31]. The cationic distribution directly relates to the degree of inversion in spinel structure [32] and is generally explained in terms of variations of oxygen vacancies [33], magneto-crystalline anisotropy [34] or a consequence of external pressure [35] but lacks a comprehensive narrative.

In this manuscript we have addressed this cationic distribution conundrum and have related it with electrochemical behavior of the cations within the spinel crystal lattice. For this purpose, nickel ions in nickel aluminate were substitutionally doped in small amounts with cobalt. The spinel crystal structure of $Ni_{1-x}Co_xAl_2O_4$ (where x = 0.01, 0.03 and 0.05) and symmetries therein are made sure to be

* Corresponding author.
E-mail address: arshadfarhan@hotmail.com (M.A. Farhan).

https://doi.org/10.1016/j.heliyon.2024.e30181
Received 4 December 2023; Received in revised form 1 April 2024; Accepted 22 April 2024
Available online 30 April 2024

kept intact with these stoichiometric variations in order to rule out effects of changing lattice and possible point defects. Owing to its similar ionic radii [36] but substantially different valence electronic structure as that of Ni, low concentration substitutional doping of Co for generating electronic perturbation without disturbing the crystal structure is opted. Structural (X-ray diffraction), electrical (Impedance Spectroscopy) and magnetic analysis are utilized to ascertain the effect of cobalt's ambivalent oxidation state on cationic distribution in nickel aluminate matrix.

2. Experimental

In Present research work, pure Crystalline phase of $NiAl_2O_4$ was synthesized by using the normal strike co-precipitation method [18] which is found most suitable for NiO free crystalline phase (Supplementary information). As reported elsewhere [37], co-precipitation method is ideal for uniform size distribution. The procedure includes mixing stoichiometric ratios of nickel nitrate hexahydrate [$Ni(NO_3)_2.6H_2O$] and aluminum nitrate nonahydrate [$Al(NO_3)_3.9H_2O$] in deionized water. The cationic solutions were mixed together under strong stirring at 60 °C for 30 min after which 10 ml of reaction medium (33 % ammonium hydroxide) was drop-wise introduced during vigorous stirring (800 rpm) for another 45 min.

The greenish-blue precipitates were separated by centrifuging the reaction mixture and subsequently washed with deionized water until neutral pH before drying overnight at 60 °C. The dried precipitates were ground into powder and calcined at 1100 °C for 12 h. For doped samples, 1 %, 3 % and 5 % of total weight was calculated and respective amount of nickel nitrate was substituted with cobalt nitrate hexahydrate [$Co(NO_3)_2.6H_2O$] to introduce Co-doping in nickel aluminate lattice and samples were labeled accordingly.

Powder X-ray diffraction was measured for crystal structure determination using Rigaku DMAX-III with Cu-Kα radiations generated at 35 kV (30 mA) in the 2θ range of 10°–80°. In order to establish the purity of $NiAl_2O_4$ crystalline phase, all diffraction patterns were subjected to Rietveld [38] fitting based on pseudo-voigt profile as implemented in Rietica software package [39] using *Fd3m* (227) cubic space group with the origin at (1/2, 1/2, 1/2) and reported structural parameters [40]. Careful refinement of occupancies ensured to balance the oxygen vacancies with minimum divergence of fitting (goodness of fit).

The electric/dielectric properties were measured via Electrochemical Impedance Spectroscopy by using Alpha-N High Resolution Dielectric Analyzer (NovoControl, Germany). Circular pallets of 10 mm diameter were pressed using 3 mg sample powder which were subsequently heat treated at 600 °C (3 h) to improve the grain-to-grain contact and mechanical stability of pallet. Contacts were made on opposite sides of pallets using silver paint and copper wires and cured at 150 °C for 2 h. Impedance response to applied AC signal (50Hz–500 kHz) was recorded with a perturbation of 0.5V and fitting for equivalent circuits was performed with Z-view software.

Lakeshore 7400 Vibrating sample magnetometer (VSM) is used to study the magnetic behavior of pure and Co-doped samples at

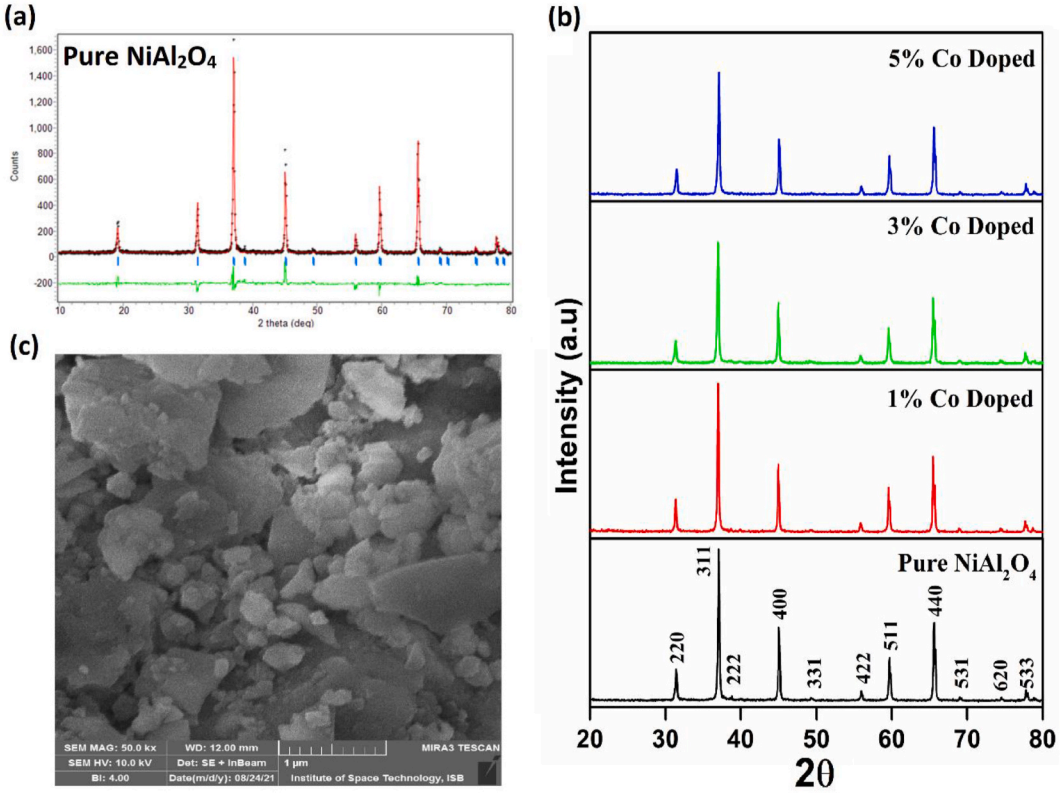

Fig. 1. (a) Rietveld fitting of $NiAl_2O_4$, (b) powder diffraction pattern for synthesized samples and (c) SEM image of synthesized material.

room temperature.

3. Results and discussion

The Rietveld analysis revealed pure crystalline partially-inverse-spinel structure of $NiAl_2O_4$ as shown in Fig. 1a. Table 1 summarizes the fitted lattice parameters with *Fd3m* symmetry accurate to third decimal place with the reported value [40]. The cell volume of 521.8 $Å^3$ and density of the sample (4.496 g/cm^3) is also found in accordance to reported value of 4.499 g/cm^3 (ISCD#06277). Analysis shows that this partially-inverse-spinel structure has both Nickel and Aluminum ions at the tetrahedral or T_d [8a] as well as octahedral or O_h [16d] sites giving it a complicated charge distribution. Owing to fast cationic self-diffusion, $NiAl_2O_4$ is reported to show varying degree of inversion in spinel lattice originating from either external or chemical pressure [35]. Such distribution can be attributed to presence of a combination of Ni^{+2}/Ni^{+3} & Al^{+2}/Al^{+3} ions instead of a divalent O_h occupancy in conventional inverse-spinel [23]. This cation distribution is further convoluted when small amount of ambivalent cobalt (Co^{+2}/Co^{+3}) is introduced to produce chemical pressure perturbation in the lattice. Additionally, owing to relatively smaller difference in the sizes of Co^{+2} and Ni^{+2} ions [36], no major structural deformation within Nickel Aluminate lattice is observed in powder diffraction patterns of doped samples (Fig. 1b) as opposed to the established fact that lattice parameters tend to change with doping of ambivalent cations in spinels [41]. The Rietveld fitting of the doped samples therefore also confirms the absence of any second phase peak thereby confirming the cation distribution conundrum. Since Ni^{+2} is reported to be more diffusive than Ni^{+3} in $NiAl_2O_4$ [42], it can be predicted that the divalent nickel ions prefer the O_h sites while the doped Co^{+2} ions from the ambivalent mix preferentially sit at T_d position that cause stretch in the partially-inverse spinel lattice nudging it towards slight increase in lattice parameters. But as the concentration of cobalt increases, it tends to occupy both T_d as well as O_h positions in the lattice. Co^{+3} ions replacing larger Ni^{+3} ions at O_h position shrink the lattice a little. Younas et al. also reported such decrease in spinel lattice parameters to be associated with increased degree of inversion in partially-inverse spinels [43]. Further doping of cobalt contributes to re-normalize the cationic distribution at the O_h site thereby expanding the lattice again. This also confirms earlier report of decreasing degree of inversion with increase in lattice parameter [35]. As reported earlier, 311 peak is most sensitive to this cationic shifting in the sub-lattice which is also observed in this study [23]. Hence; doping an ambivalent cobalt in $NiAl_2O_4$ changes the degree of inversion in the already complex partially-inverse spinel structure. Fig. 1c shows the FE-SEM micrograph of the synthesized $NiAl_2O_4$. It can clearly be observed that the irregular shaped particles have at least one nanoscale dimension. Sundaresan et al. [44] have reported that in the lower dimensional regimes, otherwise non-magnetic oxides tend to exhibit weak ferromagnetism, therefore a narrow magnetic hysteresis is expected.

The literature shows that the Nickel Aluminate has very low mobility carriers due to strictly localized charged species showing polaron hoping mechanism [12]. Such behavior can easily be explained with the help of Maxwell-Wegner model [45]. According to this model, the overall conductivity depends upon the well conducting grain (Bulk or Grain interior) and poorly conducting grain boundaries (Inter grain), respectively. Since our samples have a complex cationic distribution involving both di- and trivalent moieties of the same element, the periodic lattice within grain interior consists of strained regions where ambivalence oxidation states of Nickel, Aluminum and cobalt come into play. These regions or domains inside the bulk (grain) resonate at slightly different AC signal and thus are treated as discrete sections similar to volume defects by the hyper-sensitive Impedance spectroscopy technique. This reasoning is strengthened from the fitting of equivalent electrical circuit model to the measured data which gives at least two distinct circuit elements for best fit as shown in Fig. 2b. These two elements are argued to represent the two competing crystallographic phases of inverse and normal spinel structures respectively.

Table 2 shows the best fitting parameters for equivalent electrical circuit model with reduced chi square (χ^2) value in the range of 10^{-5} for all samples indicating goodness of fitting. It is well established [46] that the fitted capacitor value in equivalent circuit model of the order $\sim 10^{-12}$ F & $\sim 10^{-11}$ F originates from the bulk of grain and interfaces respectively. As It can be observed from the table that all capacitance values for pure $NiAl_2O_4$ range in the order of $\sim 10^{-12}$ F indicating that both circuit element represent resonance taking place inside bulk of grain. Substituting very low concentration of nickel with cobalt acts as a chemical perturbation without changing the overall crystal lattice. Therefore, the 1 % Co-doped sample show an increase in capacitance by an order of magnitude indicating changing of bulk into interface region in one of the two circuit elements. Such behavior is established to be a result of combination of di- and trivalent ions from all ionic species in the lattice [23]. The variation in the capacitance is mainly observed in the first circuit element representing inverse spinel structure while the second circuit element expressing the normal spinel structure remains unaffected although it does show small fluctuation in the overall resistance of that phase. This inference further consolidates our previous conjecture of multiple ambivalence-cationic domains within the grain. For 1 % doped samples, the capacitance of constant phase element is of the order of $\sim 10^{-11}$ implying that at very low concentration of Co, it creates sort of cationic-interfaces around these domains inside the bulk where the cations are eventually redistributed with increase in Co doping. It should be noted that higher cobalt concentration samples (5 % doping) show a similar response as that of pure $NiAl_2O_4$ signifying normalization of lattice

Table 1
Fitted Parameters of pure and Co-doped Nickel Aluminates.

Sample	Lattice parameter (Å)	R_p	R_{wp}	GOF
Pure	8.0507	11.66	14.66	1.210
1 % Co doped	8.0542	11.32	14.49	1.203
3 % Co doped	8.0509	11.21	14.18	1.082
5 % Co doped	8.0525	11.36	14.23	1.081

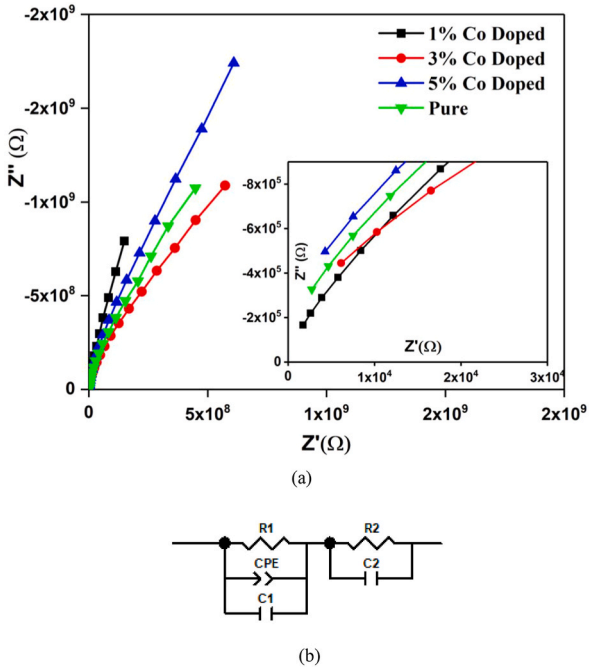

Fig. 2. (a) Impedance plain plot of pure and Co- Doped samples. Inset shows the zoomed in view of plot. (b) Fitted equivalent electrical circuit model.

Table 2
Fitting parameters for equivalent electrical circuit.

Sample	R_1 (Ω)	C of CPE (F)	n	C_1 (F)	R_2 (Ω)	C_2 (F)	χ^2
Pure	8.76×10^8	1.93×10^{-12}	0.55	1.53×10^{-12}	8.51×10^9	3.03×10^{-12}	0.12×10^{-5}
1 % Co Doped	4.53×10^9	2.40×10^{-11}	0.56	3.50×10^{-12}	1.94×10^{10}	4.70×10^{-12}	9.61×10^{-5}
3 % Co Doped	1.04×10^9	1.41×10^{-12}	0.58	9.64×10^{-13}	7.41×10^9	3.17×10^{-12}	6.87×10^{-5}
5 % Co Doped	9.05×10^8	1.38×10^{-12}	0.56	1.13×10^{-12}	1.26×10^{10}	1.66×10^{-12}	5.19×10^{-5}

towards redistributed partially-inverse spinel structure. This may be interpreted in terms of Co^{+2}/Co^{+3} system replacing Al^{+2}/Al^{+3} exchange mechanism. Fig. 2a shows the impedance plain plot (Nyquist plot) for the measured samples. The slope hints at a large apparent-semicircle which is convoluted/superimposed result of normal as well as inverse cationic-domains within the lattice grain (bulk). Form inset of Fig. 2a, it is also clear that the high frequency side of the curves do not pass through the origin indicating existence

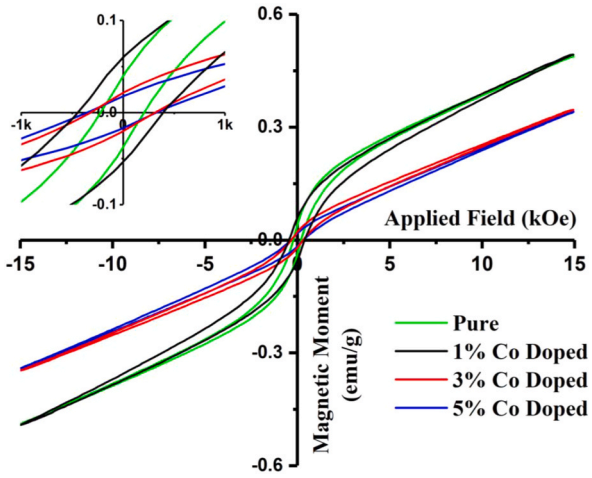

Figure: 3. Magnetic Hysteresis for pure and doped $NiAl_2O_4$.

of other relaxations beyond measuring range of the instrument.

From the trends of the semicircular arcs, it can be deduced that the lowest doped sample (1 %) has the smallest overall diameter of extrapolated semicircle implying that its impedance is least of all including pure $NiAl_2O_4$. The most probable reason is the preference of smaller cobalt ions to occupy T_d positions rendering the Ni^{+3}/Ni^{+2} and Al^{+3}/Al^{+2} electron super-exchange coupling intact at O_h sites thereby supplying more charge carriers for conduction. Increasing cobalt substitution invokes the ambivalent behavior to introduce Co^{+2}/Co^{+3} exchange system in the material. This accordingly gives rise to double exchange interactions reducing the conductivity as evident from reduced slop. At higher frequency end, the semicircular arcs are depressed to approximately a similar amount except for 3 % doped which suggest a different type of distributive element having more than one relaxation time due to ambivalence cationic-domains in the lattice. The depression angle signifies the deviation from pure/ideal capacitor behavior which is accommodated in the form of constant phase element (CPE) in the equivalent circuit model. CPE is related to capacitance by $C{=}R^{(1-n)/n}(CPE)^{1/n}$ as reported elsewhere [47]. The value of "n" gives the deviation from ideal capacitor behavior having maximum value of 1 for pure capacitive and 0 for pure resistive components. Table 1 highlights the fitted parameters on the equivalent circuit model showing smallest value of "n" for 3 % doped sample with largest depression angle (12.89°).

Magnetic measurements of pure and Co-doped samples were carried out at room temperature by using vibrating sample magnetometer (Lakeshore 7400) within the field range of ±1.5 T. Fig. 3 shows that the pure as well as doped samples form characteristic S shaped narrow hysteresis similar to the weak ferromagnetic results reported by Jayasree et al. [48]. It is pertinent to add that the shape and size of the hysteresis strongly depends upon preparation method of $NiAl_2O_4$. According to Néel's model [49] for spinel structure, magnetization of Td sites are anti-parallel to the magnetization of Oh sites partially canceling each other. The resulting magnetization is a difference of magnetic moment between Oh and Td sites (M = μB-μA) [50]. Han et al. [27] reported that $NiAl_2O_4$ is antiferromagnetic (AFM) with slightly frustrated spins. This magnetically frustrated spin structure is similar to the canted spin ferrimagnetism of homologous $NiFe_2O_4$ [43] observed at the defect boundaries and tend to vary with degree of inversion in spinel lattice. Additionally, the theoretical investigation by Elias et al. [51] suggests $NiAl_2O_4$ to have antiferromagnetic arrangement for optimized Hubbard U through van der Waals's (optB88-vdW) and Hybrid (HSE06) Potentials. Therefore, we can argue that an incomplete compensation of magnetization exists in $NiAl_2O_4$ giving it ferrimagnetic structure.

The super-exchange coupling arising from cationic distribution discussed above is also known to result in AFM arrangements confirming our previous conjecture. The AFM ground state combined with magnetically frustrated spins acts as pair of co-existing phases where interface is pinned in the backdrop of normal spinel cationic domains. Introduction of cobalt in the system provides $NiAl_2O_4$ with small number of loosely held magnetically frustrated spins near the cationic-domain interfaces which in the presence of applied magnetic field re-align to enhance overall ferrimagnetic behavior of the lattice as observed by the relatively broadened hysteresis loop. A further increase of cobalt seems to substitute the Al^{+2}/Al^{+3} system thereby highlighting the paramagnetic nature of dilute magnetic system as reported by Chen et al. [52] which can be seen from the reducing slope and coercive strength at higher cobalt concentrations.

It is well known that overall magnetization of spinel lattice is increased by increasing the magnetic moment at O_h (octahedral) or decreasing the magnetic moment at T_d (tetrahedral). So the cation distribution within spinel lattice holds the key to tune the magnetic properties of a substance. There are two unpaired electrons of Ni^{+2} ions while Co^{+2} have 3 unpaired electrons which makes substitution of Ni^{+2} with Co^{+2} more magnetic. The relatively larger Co^{+2} preferably occupy O_h thereby increasing the overall magnetization (M_s) as tabulated in Table 3. As the concentration of cobalt increases, the added cobalt occupies T_d sites in place of Al^{+2} pushing it in Al^{+3} oxidation state with a partial paramagnetic (PM)/superparamagnetic behavior and the hysteresis loop tends to show a competition of AFM and PM phases.

It can be observed from the table that the coercivity H_c values related to magneto-crystalline anisotropy or difficulty of magnetization in certain direction within crystal lattice also vary with cobalt concentration. We argue that this variation of coercivity is also a proof of cationic-domains within the bulk crystal lattice. Introduction of very small amount of Co^{+2}/Co^{+3} ions in the material disturbs the cationic distribution within the bulk and interfaces of normal and inverse spinel becomes dominant thereby increasing magnetization and hence anisotropy. With increasing Co^{+2}/Co^{+3} ions, the cationic distribution is rearranged and consequently cationic-domain structure is again stabilized with expulsion of Al^{+2} ions from octahedral sites in inverse spinel arrangement. The anisotropic constant (**K**) calculated from the formula $H_c = 0.96K/M_s$ [53] also conforms with our conclusion of rearrangement of cationic-domain structure.

Fig. 4a shows the change in AC conductivity with respect to the frequency at different concentration of cobalt doping. As discussed above, the general trend of conductivity can be explained via Maxwell-Wegner model which suggests that at lower frequency, poorly conducting grain boundaries; in our case cationic-domain-interfaces; are active that in turn lead to very low conductance and at higher frequency range the conducting grain; in our case cationic-domains within bulk/grain; become active that shows heightened conductivity. This conduction takes place through polaron hopping [12] and can further be divided into two types namely inter-well

Table 3
Magnetic Characteristics of the pure and Co doped $NiAl_2O_4$.

Sample	Coercivity	Saturation Magnetization (M_s)	Remnant Magnetization (M_r)	Squareness Ratio ($R = M_r/M_s$)	Anisotropic Constant (K)
Pure	214.48	0.48763	38.28×10^{-3}	0.078	108.9
1 % Co Doped	443.0716	0.49218	56.68×10^{-3}	0.115	227.1
3 % Co Doped	317.18	0.34637	20.82×10^{-3}	0.060	114.4
5 % Co Doped	339.12	0.34037	17.29×10^{-3}	0.050	120.2

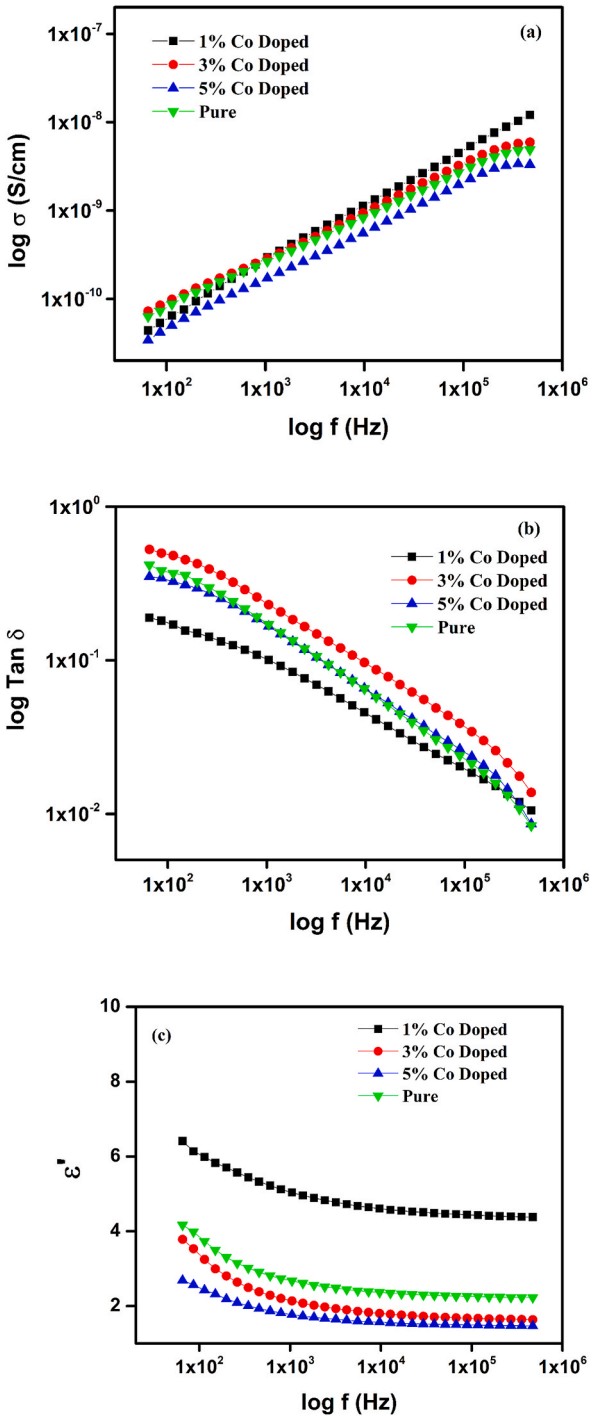

Fig. 4. (a) Conductivity, (b) tangent loss and (c) dielectric response of the pure and doped samples as a function of frequency.

hopping that occurs between two adjacent defect-wells and intra-well hoping of charge carrier within a potential well (defect) accounting for the DC portion of conductivity. The inter-well hoping follows the AC field at low frequency that leads to the dielectric relaxation and as the frequency increases; intra-well hoping becomes major contributor. At higher frequency levels, field reversal occurs very rapidly and polarons don't have enough time for long range hoping before the direction of field reverses and thus the dielectric constant at higher frequency almost becomes constant. Additionally, the polarization originating from ions has a characteristic of electronic relaxation inside grain [26] observed as a broad peak in tangent loss against frequency spectrum. In the case of material under study, we argue that the interior of grain is further sectioned into cationic-domains which have essentially the same

lattice arrangement but vary in terms of oxidation state of the certain cations constituting the partially-inverse spinel structure. Since the material has a group of such cationic domains in a crystal grain, it is expected to see more than one, merged broad peaks in the tanδ versus frequency plot. Fig. 4b shows the tanδ verses frequency plot highlighting merged/convoluted peaks which represent relaxations taking place within grain as described by Mo et al. [26].

Similarly, the dielectric response shown in Fig. 4c has a profile analogous to compact nano structured ceramic oxides [26]. It is quite apparent that despite the similarity of plot, 1 % Co doped sample has higher value of dielectric constant then other samples. This behavior can be attributed to cationic-domain-interfaces that emerge due to chemical pressure from doping of Co^{+2}/Co^{+3} in low amount. These interfaces act as dielectric medium thereby enhancing the overall permittivity of the material. Further increasing cobalt doping rearrange the cationic distribution as larger cobalt ions distributed between T_d and O_h sites within grain structure further reducing the interfacial volume. This in turn reduces the permittivity values again but owing to blockage of super exchange in Al^{+2}/Al^{+3} system, it's value is still larger than the pure $NiAl_2O_4$. It is interesting to note that although the partial-inversion of spinel structure has been known to have varying cationic distribution, this report presents the first ever observation offering an explanation on the subject.

4. Conclusion

Nickel Aluminate with cobalt substitutional doping was synthesized with partially inverse spinel structure and compared to the published literature. The cationic distribution in the partially-inverse spinel structure is correlated with the cationic-domains within the lattice which are identified as regions in the bulk having same lattice arrangement but different cationic oxidation states (normal and inverse spinel lattice). The inconclusive dielectric behavior reported in literature is hereby suggested to originate from this cationic domain structure inside the bulk. The results show that the cationic distribution is changed by perturbing the system with introduction of low concentrations of ambivalent substituents while keeping the same lattice arrangement within the crystal. This tunability of domain structure is deduced with the supported by crystal structure analysis, electrochemical impedance spectroscopy and magnetization measurements.

CRediT authorship contribution statement

M. Arshad Farhan: Writing – review & editing, Supervision, Conceptualization, Formal analysis, Methodology. **Sadaf Javaid:** Writing – original draft, Formal analysis, Data curation. **Lubna Rasheed:** Supervision, Project administration. **M. Atiq Ur Rehman:** Data curation. **M. Nadeem:** Validation, Supervision.

Declaration of competing interest

The authors declare that they have no known competing financial interests or personal relationships that could have appeared to influence the work reported in this paper.

Acknowledgment

The authors would like to acknowledge Dr. M. Younas (Late) and Dr. Rao Tahir Ali Khan for their useful discussions on electrochemical impedance and crystal structure analysis respectively.

Appendix A. Supplementary data

Supplementary data to this article can be found online at https://doi.org/10.1016/j.heliyon.2024.e30181.

References

[1] B.P. Uberuaga, Intricate disorder, Nat. Mater. 15 (5) (2016) 496–497.
[2] M. George, T.L. Ajeesha, A. Manikandan, A. Anantharaman, R.S. Jansi, E.R. Kumar, et al., Evaluation of Cu–$MgFe_2O_4$ spinel nanoparticles for photocatalytic and antimicrobial activates, J. Phys. Chem. Solid. 153 (2021) 110010.
[3] T. Tatarchuk, L. Soltys, W. Macyk, Magnetic adsorbents for removal of pharmaceuticals: a review of adsorption properties, J. Mol. Liq. 384 (2023) 122174.
[4] C.A. Paul, E.R. Kumar, J. Suryakanth, A.F.A. El-Rehim, Structural, microstructural, vibrational, and thermal investigations of NiO nanoparticles for biomedical applications, Ceram. Int. 49 (16) (2023) 27230–27246.
[5] C. Arun Paul, E. Ranjith Kumar, A.F. Abd El-Rehim, G. Yang, Cobalt oxide nanoparticles for biological applications: synthesis and physicochemical characteristics for different natural fuels, Ceram. Int. 49 (24, Part A) (2023) 40244–40257.
[6] T. Indumathi, A.H. Hirad, A.A. Alarfaj, E. Ranjith Kumar, K. Chandrasekaran, Phytoextract-mediated synthesis of Cu doped NiO nanoparticle using cullon tomentosum plant extract with efficient antibacterial and anticancer property, Ceram. Int. 49 (19) (2023) 31829–31838.
[7] N.Y. Elamin, T. Indumathi, E. Ranjith Kumar, Pluronic f127 encapsulated titanium dioxide nanoparticles: Evaluation of physiochemical properties for biological applications, J. Mol. Liq. 379 (2023) 121655.
[8] J. Guo, H. Lou, H. Zhao, D. Chai, X. Zheng, Dry reforming of methane over nickel catalysts supported on magnesium aluminate spinels, Appl. Catal. Gen. 273 (1) (2004) 75–82.
[9] K.L. Scrivener, J.-L. Cabiron, R. Letourneux, High-performance concretes from calcium aluminate cements, Cement Concr. Res. 29 (8) (1999) 1215–1223.

[10] P. McMillan, B. Piriou, A. Navrotsky, A Raman spectroscopic study of glasses along the joins silica-calcium aluminate, silica-sodium aluminate, and silica-potassium aluminate, Geochem. Cosmochim. Acta 46 (11) (1982) 2021–2037.
[11] K.S. Suresh, D.G. Kanhere, P. Ravindra, Electronic structure of spinel oxides: zinc aluminate and zinc gallate, J. Phys. Condens. Matter 11 (18) (1999) 3635.
[12] S. Kurien, J. Mathew, S. Sebastian, S.N. Potty, K.C. George, Dielectric behavior and ac electrical conductivity of nanocrystalline nickel aluminate, Mater. Chem. Phys. 98 (2) (2006) 470–476.
[13] J.N. Roelofsen, R.C. Peterson, M. Raudsepp, Structural variation in nickel aluminate spinel ($NiAl_2O_4$), Am. Mineral. 77 (5–6) (1992) 522–528.
[14] L. Kou, J.R. Selman, Activity of $NiAl_2O_4$ Catalyst for Steam reforming of methane under internal reforming fuel cell conditions, ECS Proceedings Volumes 1999–19 (1) (1999) 640.
[15] L. Kou, J.R. Selman, Electrical conductivity and chemical diffusivity of $NiAl_2O_4$ spinel under internal reforming fuel cell conditions, J. Appl. Electrochem. 30 (12) (2000) 1433–1437.
[16] K.E. Sickafus, N. Yu, M. Nastasi, Radiation resistance of the oxide spinel: the role of stoichiometry on damage response, Nucl. Instrum. Methods Phys. Res. Sect. B Beam Interact. Mater. Atoms 116 (1) (1996) 85–91.
[17] J.W. Kim, P.W. Shin, M.J. Lee, S.J. Lee (Eds.), Effect of Particle Size on the Strength of a Porous Nickel Aluminate Fabricated by a Polymer Solution Route, 2006.
[18] M. Hasan, J.W. Drazin, S. Dey, R.H.R. Castro, Synthesis of stoichiometric nickel aluminate spinel nanoparticles, Am. Mineral. 100 (2015) 652–657.
[19] D.R.K.G. Sowman, inventorMicrocrystalline Transition Metal Oxide Spinel Articles, 1988. US.
[20] P.S. Patil, R.S. Dhivare, S.R. Mirgane, B.G. Pawar, T.R. Mane, Cobalt-doped nickel aluminate nanomaterials synthesis, characterization, and catalytic properties, Macromol. Symp. 393 (1) (2020) 2000163.
[21] F.Z. Akika, M. Benamira, H. Lahmar, A. Tibera, R. Chabi, I. Avramova, et al., Structural and optical properties of Cu-substitution of $NiAl_2O_4$ and their photocatalytic activity towards Congo red under solar light irradiation, J. Photochem. Photobiol. Chem. 364 (2018) 542–550.
[22] A. Morales-Marín, J.L. Ayastuy, U. Iriarte-Velasco, M.A. Gutiérrez-Ortiz, Nickel aluminate spinel-derived catalysts for the aqueous phase reforming of glycerol: effect of reduction temperature, Applied Catalysis B: Environmental. 244 (2019) 931–945.
[23] A. Hamdedein, W.M.A. El Rouby, M.D. Khan, M.M. El-Deeb, A.A. Farghali, M.H. Khedr, et al., Synthesis and characterization of $Ni/NiCo_2O_4$ modified electrode for methanol electro-catalytic oxidation, IOP Conf. Ser. Mater. Sci. Eng. 1046 (1) (2021) 012027.
[24] B. Seo, E.H. Ko, J. Boo, M. Kim, D. Kang, N.-K. Park, CO_2 Hydrogenation on $Nix Mg_{1-x} Al_2O_4$: a Comparative study of $MgAl_2O_4$ and $NiAl_2O_4$, Catalysts 11 (9) (2021) 1026.
[25] M.A. Rahman, E. Ahamed, M.R.I. Faruque, M.T. Islam, Preparation of $NiAl_2O_4$-based Flexible Substrates for metamaterials with Negative dielectric properties, Sci. Rep. 8 (1) (2018) 14948.
[26] C-m Mo, L. Zhang, G. Wang, Characteristics of dielectric behavior in nanostructured materials, Nanostruct. Mater. 6 (5) (1995) 823–826.
[27] M. Han, Z. Wang, Y. Xu, R. Wu, S. Jiao, Y. Chen, et al., Physical properties of $MgAl_2O_4$, $CoAl_2O_4$, $NiAl_2O_4$, $CuAl_2O_4$, and $ZnAl_2O_4$ spinels synthesized by a solution combustion method, Mater. Chem. Phys. 215 (2018) 251–258.
[28] S. Karmakar, D. Behera, Non-overlapping small polaron tunneling conduction coupled dielectric relaxation in weak ferromagnetic $NiAl_2O_4$, J. Phys. Condens. Matter 31 (24) (2019) 245701.
[29] H. Agarwal, T.P. Yadav, O.N. Srivastava, M.A. Shaz, Dielectric response and alternating current conductivity in $(Co,Ni)Al_2O_4$ nano-spinel, Ceram. Int. 43 (18) (2017) 16986–16992.
[30] R.K. Datta, R. Roy, Equilibrium order-disorder in spinels, J. Am. Ceram. Soc. 50 (11) (1967) 578–583.
[31] V. Stevanović, M. d'Avezac, A. Zunger, Universal Electrostatic origin of cation ordering in A_2BO_4 spinel oxides, J. Am. Chem. Soc. 133 (30) (2011) 11649–11654.
[32] T. Tatarchuk, A. Shyichuk, J. Lamkiewicz, J. Kowalik, Inversion degree, morphology and colorimetric parameters of cobalt aluminate nanopigments depending on reductant type in solution combustion synthesis, Ceram. Int. 46 (10, Part A) (2020) 14674–14685.
[33] R.F. Cooley, J.S. Reed, Equilibrium cation distribution in $NiAl_2O_4$, $CuAl_2O_4$, and $ZnAl_2O_4$ spinels, J. Am. Ceram. Soc. 55 (8) (1972) 395–398.
[34] M. Deepty, G. Prasad, C. Srinivas, S.A.V. Prasad, E.R. Kumar, N.K. Mohan, et al., Magnetic studies of Mn^{2+} substituted Zn-ferrite nanoparticles: role of secondary phases, bond angles and magnetocrystalline anisotropy, Solid State Commun. 361 (2023) 115077.
[35] H. Itzhak, D. Danut, Ü. Ersan, F.Y. Alan, H.A. Elizabeth, H. Jingzhu, et al., The effect of pressure on the structure of $NiAl_2O_4$, J. Phys. Condens. Matter 14 (44) (2002) 10511.
[36] R.D. Shannon, Revised effective ionic radii and systematic studies of interatomic distances in halides and chalcogenides, Acta Crystallogr. A 32 (5) (1976) 751–767.
[37] D. Sudha, E.R. Kumar, S. Shanjitha, A.M. Munshi, G.A.A. Al-Hazmi, N.M. El-Metwaly, et al., Structural, optical, morphological and electrochemical properties of ZnO and graphene oxide blended ZnO nanocomposites, Ceram. Int. 49 (5) (2023) 7284–7288.
[38] H.M. Rietveld, Line profiles of neutron powder-diffraction peaks for structure refinement, Acta Crystallogr. 22 (1967).
[39] Rietica - a visual Rietveld program, in: B.A. Hunter (Ed.), 2nd AINSE Symposium on Neutron Scattering Powder Diffraction and Australian Neutron Beam Users Group Meeting Symposium Handbook, 2000. Australia).
[40] Y.S. Han, J.B. Li, X.S. Ning, B. Chi, Effect of preparation temperature on the lattice parameter of nickel aluminate spinel, J. Am. Ceram. Soc. 87 (7) (2004) 1347–1349.
[41] S.A.V. Prasad, C. Srinivas, R. Jeevan Kumar, E. Ranjith Kumar, K. Vijaya Babu, S.S. Meena, et al., Study of thermal, structural, microstructural, vibrational and elastic properties of $Mn_xMg_{0.8-x}Zn_{0.2}Fe_2O_4$ ($0.1 \leq x \leq 0.7$) ferrite nanoparticles, Ceram. Int. 49 (12) (2023) 20419–20428.
[42] N.M. Deraz, Synthesis and characterization of nano-Sized nickel aluminate spinel crystals, Int. J. Electrochem. Sci. 8 (4) (2013) 5203–5212.
[43] M. Younas, M. Nadeem, M. Atif, R. Grossinger, Metal-semiconductor transition in $NiFe_2O_4$ nanoparticles due to reverse cationic distribution by impedance spectroscopy, J. Appl. Phys. 109 (9) (2011).
[44] A. Sundaresan, R. Bhargavi, N. Rangarajan, U. Siddesh, C.N.R. Rao, Ferromagnetism as a universal feature of nanoparticles of the otherwise nonmagnetic oxides, Phys. Rev. B 74 (16) (2006) 161306.
[45] J.C. Maxwell, A Treatise on Electricity and Magnetism, Cambridge University Press, Cambridge, 2010.
[46] J.T.S. Irvine, D.C. Sinclair, A.R. West, Electroceramics: characterization by impedance spectroscopy, Adv. Mater. 2 (3) (1990) 132–138.
[47] Evgenij Barsoukov, J.R. Macdonald, Impedance Spectroscopy: Theory, Experiment, and Applications, third ed. ed, John Wiley & Sons, Inc., 2018.
[48] S. Jayasree, A. Manikandan, S.A. Antony, A.M. Uduman Mohideen, C. Barathiraja, Magneto-Optical and catalytic properties of Recyclable spinel $NiAl_2O_4$ Nanostructures using facile combustion methods, J. Supercond. Nov. Magnetism 29 (1) (2016) 253–263.
[49] A.A. Ati, Z. Othaman, A. Samavati, Influence of cobalt on structural and magnetic properties of nickel ferrite nanoparticles, J. Mol. Struct. 1052 (2013) 177–182.
[50] S. Debnath, A. Das, R. Das, Effect of cobalt doping on structural parameters, cation distribution and magnetic properties of nickel ferrite nanocrystals, Ceram. Int. 47 (12) (2021) 16467–16482.
[51] I. Elias, A. Soon, J. Huang, S.H. B, A. Montoya, Atomic order, electronic structure and thermodynamic stability of nickel aluminate, Phys. Chem. Chem. Phys. 21 (47) (2019) 25952–25961.
[52] X. Chen, S. Bedanta, O. Petracic, W. Kleemann, S. Sahoo, S. Cardoso, et al., Superparamagnetism versus superspin glass behavior in dilute magnetic nanoparticle systems, Phys. Rev. B 72 (21) (2005) 214436.
[53] C. Srinivas, M. Deepty, S.A.V. Prasad, G. Prasad, E.R. Kumar, S.S. Meena, et al., Study of structural, vibrational, elastic and magnetic properties of uniaxial anisotropic Ni-Zn nanoferrites in the context of cation distribution and magnetocrystalline anisotropy, J. Alloys Compd. 873 (2021) 159748.